

Article

Development of a Poppet-Type Pneumatic Servo Valve

Takahiro Kanno ^{1,†} , Takashi Hasegawa ^{1,†}, Tetsuro Miyazaki ¹, Nobuyuki Yamamoto ²,
Daisuke Haraguchi ² and Kenji Kawashima ^{1,*}

¹ Tokyo Medical and Dental University, 2-3-10, Kanda Surugadai, Chiyoda-ku, Tokyo 101-0062, Japan; kanno.bmc@tmd.ac.jp (T.K.); drivevolleyer@gmail.com (T.H.); tmiyazaki.bmc@tmd.ac.jp (T.M.)

² RiverField Inc., Yotsuya Medical Bldg. 5th floor, 20 Samon-cho, Shinjuku-ku, Tokyo 160-0017, Japan; n-yamamoto.rfc@riverfieldinc.com (N.Y.); d-haraguchi.rfc@riverfieldinc.com (D.H.)

* Correspondence: kkawa.bmc@tmd.ac.jp; Tel.: +81-3-5280-8163

† These authors contributed equally to this work.

Received: 10 October 2018; Accepted: 30 October 2018; Published: 31 October 2018



Abstract: In pneumatic positioning and force-control systems, spool-type servo valves are widely used for obtaining quick responses and precise control. However, air leakage from these valves results in increased energy consumption. To address this problem, we developed a three-port poppet-type servo valve to reduce air leakage. The developed valve consists of a camshaft, two orifices, two metal balls, and a housing with two flow channels. The metal ball is pushed by fluid, and spring force closes the orifice. The port opens when the cam rotates and pushes the ball. The cam shape and orifice size were designed to provide the desired flow rate. The specifications of the DC motor for rotating the camshaft were determined considering the fluid force on the ball. Static and dynamic characteristics of the valve were measured. We experimentally confirmed that air leakage was 0.1 L/min or less. The ratio of air leakage to maximum flow rate was only 0.37%. Dynamic characteristic measurements showed that the valve had a bandwidth of 30 Hz. The effectiveness of the valve was demonstrated through experiments involving pressure and position control.

Keywords: servo valve; pneumatics; position control

1. Introduction

Recently, pneumatic servo systems have been widely adopted for use in robotic systems and vibration-isolation devices. The use of air in such applications has several advantages, including the nonmagnetism of air, the achievement of high power-to-weight ratios, and reduced heat generation. Pneumatic servo valves are a key element in pneumatic servo systems. The characteristics of these valves are a critical factor in achieving satisfactory performance [1–5]. There are mainly two types of pneumatic servo valve: the nozzle-flapper type, and the spool type. Nozzle-flapper type servo valves can directly control pressure. The pressure-control systems associated with the valves are generally approximated to a first-order lag system assuming an isothermal state change for the air in the load chamber [6,7]. These valves have both high responsiveness and high linearity. However, they require high exhaust flow rates in order to provide the precise control of pressure.

Spool-type servo valves can directly control flow rate. Because their exhaust flow rates are smaller than those of nozzle-flapper type valves, spool-type servo valves are widely used in pneumatically driven robot systems [8–10]. However, spool-type valves still experience air leakage owing to the presence of a gap between the spool and the sleeve. Usually, leakage flow is approximately 3% to 5% of the maximum flow rate. With the commercialization of servo valves, it is highly desirable to decrease exhaust flow rates in order to reduce energy consumption and operating costs.

To overcome this problem, poppet-type [11] and pinch-type valves [12–14] have been developed. Most of these valves only have two ports. The valve shown in Reference [14] has three ports, but the overlap condition should be improved. Three-port poppet-type servo valves had not yet been commercialized at the time of our investigation. A pneumatic cylinder can be controlled with a five-port servo valve, but two valves are required with a three-port valve. The use of three-port valves increases the cost. However, the use of two three-port valves becomes suitable for compliance control because each cylinder chamber can be individually controlled. A study [15] showed that the use of only one five-port servo valve may lead to very steep variation of the fluidic stiffness around zero velocity; independent pneumatic force control in each chamber, using two servo valves, surpasses this drawback. A zero-lap condition is desirable for precise control with three-port valves. Moreover, the dynamic response of servo valves is important for precise position control in a pneumatic servo system [16].

The purpose of this study was to develop a three-port poppet-type servo valve with high dynamic response and nearly zero lap. The target leak flow was 1% or less than the maximum flow rate. Further, to allow the valves to be used in soft robots controlled at low flow rates, maximum flow rate was designed to be less than 30 L/min. The characteristics of the valve were measured, and the effectiveness of the valve is demonstrated through pressure and position-control experiments.

The remainder of the paper is organized as follows: Section 2 describes the design of the proposed valve. The static and dynamic characteristics of the valve are discussed in Section 3, and Section 4 reports the results of the position-control experiments. Finally, the conclusions of this work are presented in Section 5.

2. Developed Valve

The proposed valve is developed to enable the control of pneumatically driven robotic forceps [10]. The required maximum flow rate is 25 L/min, as per the maximum speed of the forceps. To achieve good controllability, valve dynamics must be approximately the same as those of commercial valves. In particular, in surgical robots that must manipulate forceps for several hours during a surgical procedure, the valve leakage rate must be nearly zero in order to achieve energy savings.

2.1. Valve Structure

Figures 1 and 2 respectively show the schematic and image of the developed valve. The valve mainly consists of a camshaft, two orifices, two metal balls, and a housing with two flow channels. The valve has four ports: a supply port, an exhaust port, and two control ports. Two control ports connect to one flow path downstream of the housing. Thus, the proposed valve is functionally equivalent to general three-port valves, though it apparently has four ports. The two orifices are arranged in each flow channel. The balls are placed upstream of the orifices. When the input voltage to the motor to rotate the camshaft is zero, air flow is obstructed as the two balls are pushed into the orifices by upstream pressure and spring force. A spring with a spring constant of 0.02 N/mm was used. Two springs are placed between the ball and the washer as shown in Figure 1. The port is opened when the camshaft is rotated, and the cam at the downstream side of the orifice pushes the ball. The cost of the camshaft is about US\$650, owing to the complex shape. The costs of two orifices are about US\$300. The body of the valve is printed by a 3D printer. Other elements are relatively inexpensive. The cost of creating the valve prototype is about US\$950. However, when the valve is mass-produced, its cost may decrease by half.

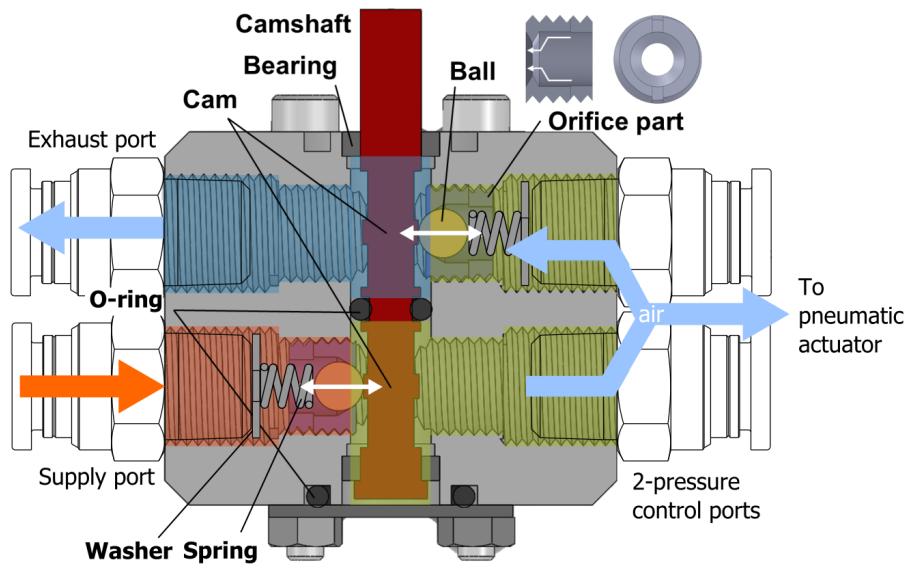


Figure 1. Schematic of poppet-type pneumatic servo valve.

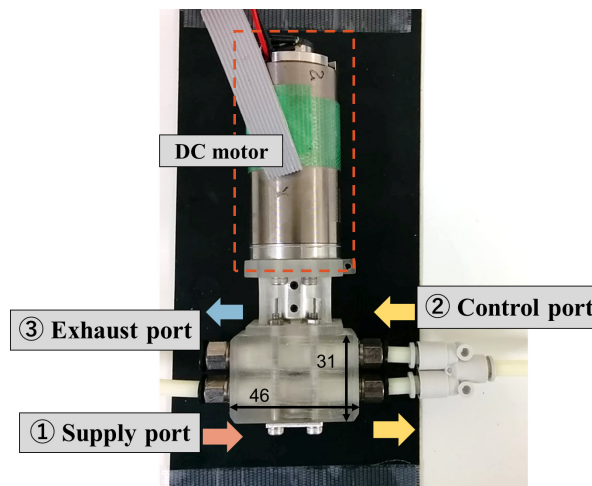


Figure 2. Photograph of the developed valve.

Figure 3 shows the arrangement of the camshaft, cams, and balls. The camshaft and cams are one element made of stainless steel. When the angle of the camshaft corresponds to the neutral position, the two balls come in contact with the orifices, thereby shutting off the flow. Thus, the initial condition of the valve is closed. Flow direction is determined by the rotational direction of the camshaft. Cams are placed on the camshaft at an initial offset angle of 30 degrees in order to prevent overlapping.

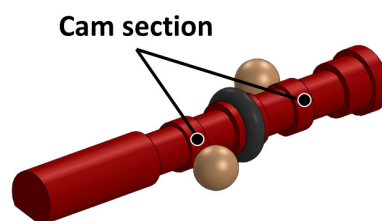


Figure 3. Arrangement of cams, camshaft, and balls.

Flow rate is controlled by the rotation angle of the camshaft. When the camshaft rotates counterclockwise, the ball at the control port is pushed to allow the exhaust port to open and discharge air. At this time, the supply port remains closed. When the camshaft rotates clockwise, the air flows

toward the control port while the exhaust port is closed. The radius of the cam is designed to linearly change the effective area of the valve with respect to the cam angle. The position of the orifice can be adjusted with screws. Therefore, the lap condition of the valve can be changed by adjusting the position of the orifice.

2.2. Orifice Design

Flow rate through the orifice is represented in the following two formulas [17]. In the case of choked flow:

$$G = K_f S_e P_s \sqrt{\frac{T_0}{T_{air}}} \quad (1)$$

In the case of subsonic flow:

$$G = K_f S_e P_s \sqrt{\frac{T_0}{T_{air}}} \sqrt{1 - \left(\frac{P_c - b}{1 - b}\right)^2} \quad (2)$$

In Equations (1) and (2), G is the flow rate, K_f is the proportional constant, S_e is the effective area, T_0 is the temperature under normal conditions, T_{air} is the temperature of the air, P_s is the supply pressure, P_c is the downstream pressure, and b is the critical ratio.

The maximum flow rate at the choked condition was determined to be 26 L/min at a supply pressure of 500 kPa. Then, maximum effective area S_e was approximately 0.45 mm² as per Equation (1). Here, $K_f = 11.1$, $T_0 = 273$ K, and $T_{air} = 293$ K. Figure 4 shows the sectional view of the orifice. The upper and lower figures, respectively, show the cross section of the orifice when the valve is shut and opened by the cam. The sectional area of valve S can be obtained geometrically according to Figure 4.

$$S = \pi \{(r + b_{max})^2 - r^2\} \sin \varphi \quad (3)$$

Here, r , b_{max} , and φ , respectively, denote the radius of the ball, the gap between the orifice and the ball, and the slope angle of the orifice, as shown in Figure 4. Gap b_{max} can be obtained by the displacement of cam y_{st} as:

$$b_{max} = y_{st} \cos \varphi. \quad (4)$$

Then, the sectional area can be calculated from Equations (3) and (4) as follows:

$$S = (2ry_{st} \cos \varphi + y_{st}^2 \cos^2 \varphi) \pi \sin \varphi \quad (5)$$

The ball surface must protrude from the orifice to be pushed by the cam. The displacement of the ball tip to orifice surface h_{out} can be described as:

$$h_{out} = r - r \cos \varphi - \left(r \sin \varphi - \frac{d_0}{2}\right) \tan \varphi. \quad (6)$$

Then, the diameter of orifice d_0 can be written as follows:

$$d_0 = 2\left(r \sin \varphi - \frac{r - r \cos \varphi - h_{out}}{\tan \varphi}\right) \quad (7)$$

The effective area of valve S_e can be obtained by multiplying Equation (5) by the contraction coefficient. The contraction coefficient of the orifices is approximately 0.85 [18]. Therefore, sectional area S becomes 0.53 mm² to satisfy the maximum flow rate of 25 L/min. First, radius r , angle φ , and the diameter of orifice d_0 were determined; they are listed in Table 1. Then, b_{max} was calculated from Equation (3), and y_{st} was obtained as 0.25 mm from Equation (4). Finally, the cam was designed to move the ball by 0.25 mm.

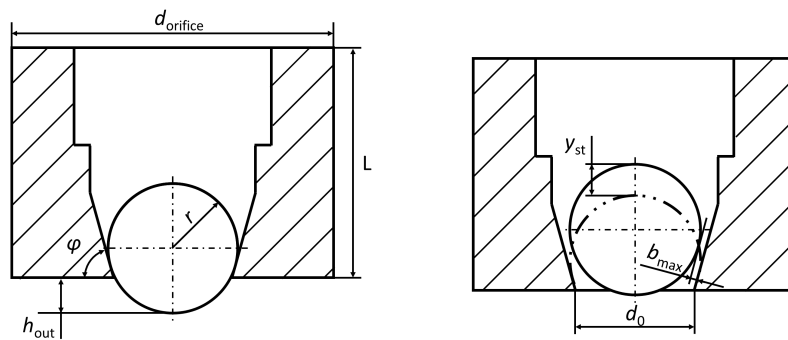


Figure 4. Sectional view of orifice part.

Table 1. Design variables of orifice parts.

Parameters	Value
Radius r	2 mm
Orifice angle φ	75 deg
Orifice diameter d_0	3.6 mm

2.3. Selection of Orifice Material

Because air viscosity is rather small compared to that of liquids, air leakage can easily occur between orifice and ball. Therefore, the selection of orifice material was an important consideration. We evaluated three materials for the orifice: aluminum, polypropylene, and polyacetal. The prototypes for the aluminum and polyacetal orifices were cut using a surface roughness of Ra 1.6. The polypropylene orifice was fabricated using a 3D printer. The air leakages at a supply pressure of 500 kPa were then measured using a flow meter.

The experimental results are shown in Table 2. Air leakage decreased when polyacetal was used owing to the elasticity of the material. Moreover, polyacetal is suitable for facilitating shutting off air flow. Therefore, polyacetal was selected as the orifice material.

Table 2. Air leakage with different orifice materials.

Materials	Value
Aluminum r	18.8 L/min
Polypropylene φ	1.0 L/min
Polyacetal. d_0	0.1 L/min

2.4. Cam Design

Figure 5 shows the designed cam shape. The left figure shows the cross-section of the cam, and the right figure shows the relation between the radius and angle of the cam. The difference between the maximum and minimum radii was set to 0.25 mm, as per the design described in Section 2.2. The cam was designed to linearly push the ball, as shown in the right figure of Figure 5. The controllable range of the cam was ± 60 deg, as the cam was placed on the camshaft at an offset angle of 30 deg from the vertical axis, as shown in the middle figure of Figure 6, in order to prevent overlapping.

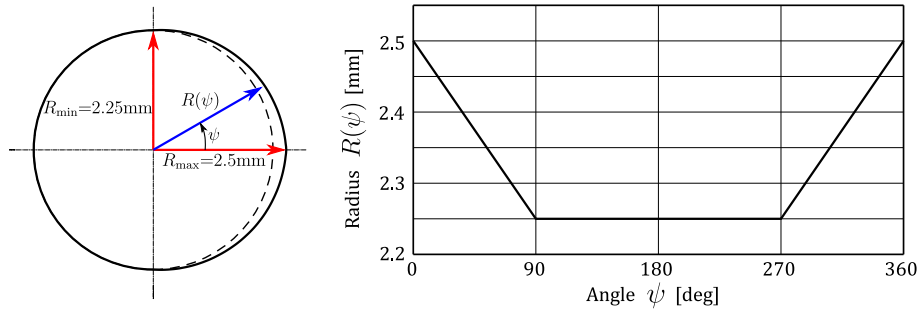


Figure 5. Designed cam shape.

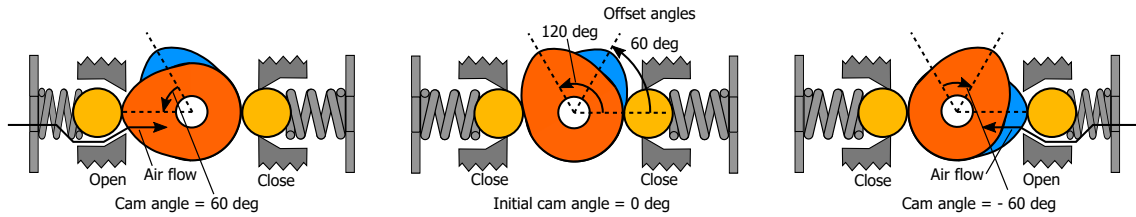


Figure 6. Cam arrangement.

2.5. Motor Selection

The camshaft must smoothly rotate to control the flow rate of the valve. The pushing and friction forces of the two cams and the O-ring act on the shaft. The torque required to push the cam, τ_c , is calculated by the principle of virtual work as follows:

$$\tau_c d\theta = (F_b + F_d) dx \tag{8}$$

Here, F_b is the pushing force of the ball, which is given as:

$$F_b = P\pi r^2. \tag{9}$$

F_b becomes 7.4 N at $P = 500$ kPa. F_d is the drag force on the ball, which is given as:

$$F_d = \frac{1}{2} \rho v^2 C_d \pi r^2. \tag{10}$$

Here, ρ is air density, v is air velocity, and C_d is the drag coefficient. Under the choked condition, velocity increases to the speed of sound. The Reynolds number is about 4600. Therefore, C_d is given as 0.47. Then, F_d becomes 0.6 N at $p = 500$ kPa. dx is the distance that the ball moves, and $d\theta$ is the rotation angle of the shaft. As a result, the torque τ_c required to push the cam for one ball is calculated as follows, as per the geometry from Figure 5, at $P = 500$ kPa.

$$\tau_c = \frac{(F_b + F_d) dx}{d\theta} = 0.02 \text{ Nm} \tag{11}$$

The torque to rotate O-ring τ_o is given as follows:

$$\tau_o = \mu F_o r_o \tag{12}$$

Here, μ , F_o , and r_o are the friction coefficient, frictional force, and radius of the O-ring, respectively. The inner diameter and thickness of the O-ring were selected as 3.5 mm and 1.9 mm, respectively, as per the size of the camshaft. The stress of the O-ring (0.25 N/mm) was obtained from the O-ring catalog. Force F_o was obtained as 4.2 N with a compression of 0.1 mm. Then, τ_o became approximately 0.03 Nm with $\mu = 1.0$. A torque of at least 0.05 Nm was required to rotate the camshaft. Valve dynamics depend on the performance of the motor. We selected a DC motor (Maxon DCX 35L) to control the valve; this

highly responsive motor, which can generate a torque of 0.12 Nm, has a mechanical time constant of 3.97 ms. The cost of the motor is about US\$350.

3. Valve Characteristics

3.1. Static Characteristics

We measured the static characteristics of the developed valve. The camshaft was connected to the DC motor, and the angle of the camshaft was controlled using a microcomputer (Arduino). We measured the flow rates by changing the rotational angles of the cam. The supply and downstream pressures were set to 500 kPa and atmospheric-pressure values, respectively.

The experimental results are shown in Figure 7. The hysteresis of the flow rate to the cam angle was small. Flow rate changed linearly with respect to the cam angle. The maximum flow rate was 27 L/min, which was almost the same as the designed value. We confirmed that the valve could achieve an almost zero-lap condition. Air leakage was 0.1 L/min or less, and the ratio of air leakage to the maximum flow rate was 0.37%. These values were fairly low compared to those of a spool-type servo valve (FESTO MPYE-5-M5-010-B), which exhibited air leakage of 1.9 L/min and a ratio of approximately 3.5%.

Then, we measured the flow characteristics of the valve using the experimental setup in accordance with the procedure recommended by ISO 6358. An experimental result with a cam angle of 40 deg is shown in Figure 8. As shown in the figure, the critical pressure ratio was 0.44 at a supply pressure of 500 kPa. The critical pressure ratios of commercially available valves are approximately 0.3 to 0.45 [17,19]. The path is geometrically symmetrical because the flow path is between the orifice and the ball. Therefore, the developed valve has a wide choke range compared with conventional valves.

Furthermore, we measured the pressure gain characteristics at zero flow. The pressure sensor was directly connected to the control port of the servo valve. The relation between the rotation angle of the cam and the pressure in the control port was measured. Figure 9 shows the results at a supply pressure of 500 kPa. We confirmed that the pressure gain was large because the valve leakage rate is small.

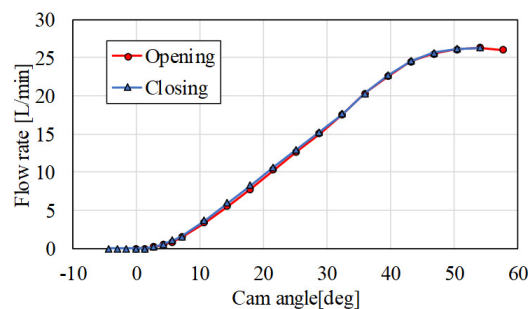


Figure 7. Static characteristics of developed valve.

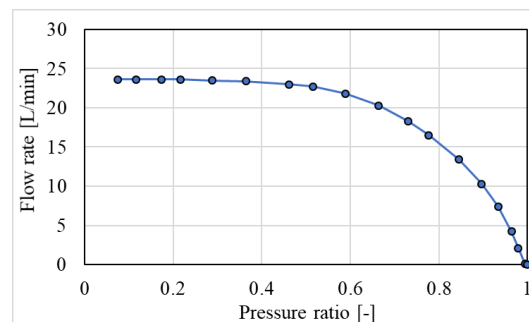


Figure 8. Flow characteristics of developed valve.

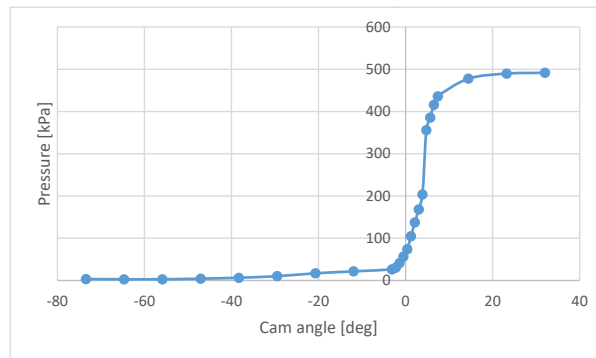


Figure 9. Pressure gain characteristics of developed valve.

3.2. Dynamic Characteristics

We executed a pressure-control experiment connecting a pressure sensor directly to the control port. During the experiment, the dead volume of $1.4 \times 10^3 \text{ mm}^3$ remained even when directly connecting the sensor to the valve.

A PI feedback controller was used for pressure control. A PC was used as the controller; the measured pressure was entered into the PC by an AD converter. The control signal was provided to the DC motor through a DA converter. A block diagram of the pressure control is shown in Figure 10. The control parameters were determined by trial and error, and are listed in Table 3. The parameters were determined to be as large as possible to minimize offset during stable conditions. In this experiment, sinusoidal reference pressures with an amplitude of 20 kPa and an offset of 200 kPa were entered into the controller. The frequency of the reference input ranged between 0.1 and 30 Hz.

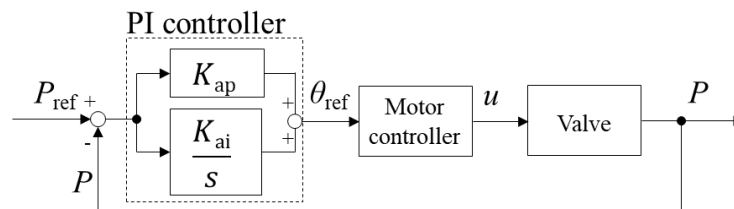


Figure 10. Block diagram of pressure control.

Table 3. Control gains of pressure control.

K_{ap}	4.0 V/kPa
K_{ai}	0.25 V/kPa s

The experimental results at frequencies of 0.1 and 5.0 Hz are shown in Figure 11. The upper figures show the pressure, and the lower figures show the cam angle. It is clear that the valve can control the pressure at a frequency of 0.1 Hz. A small phase delay is observed at a frequency of 5.0 Hz. The results were summarized in a Bode diagram, as shown in Figure 12. We confirmed that bandwidth was higher than 30 Hz when using the proposed valve. The phase lag became -180 deg at 40 Hz. This is considered to be a result of the motor dynamics. To enable comparison, we performed the same experiments using a commercially available spool-type servo valve (FESTO MPYE-5-M5-010-B), in which the maximum flow rate is approximately the same as that of the developed valve. The results for the spool-type valve are plotted in Figure 12. Up to 30 Hz, it is clear that the developed valve

demonstrated almost the same performance as the spool-type servo valve. The dynamic response could be improved by changing the DC motor to one having a higher response.

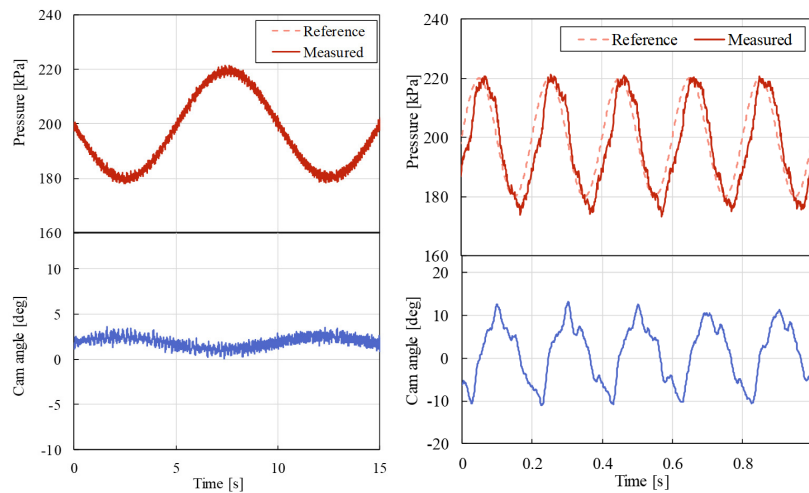


Figure 11. Results of pressure control (left: 0.1 Hz, right: 5.0 Hz).

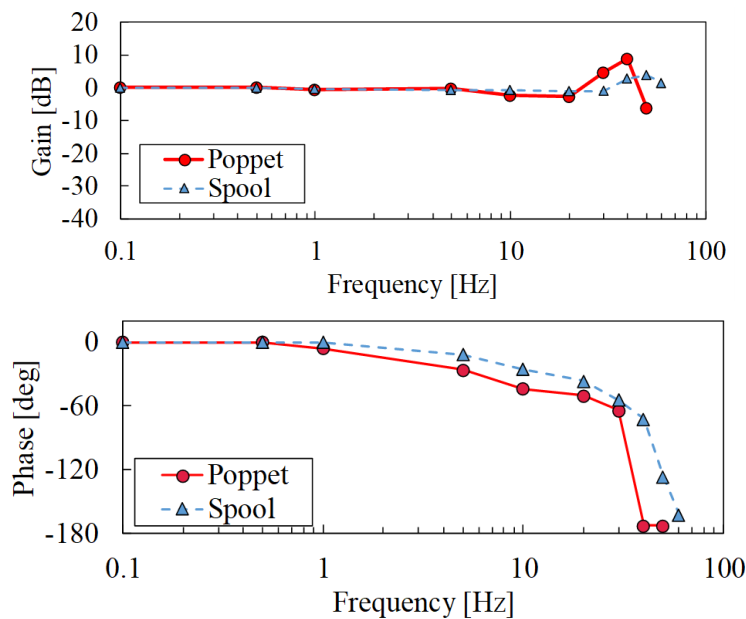


Figure 12. Frequency response of pressure control.

4. Position Control of Pneumatic Cylinder Using the Developed Valve

We executed a position-control experiment using a low-friction-type pneumatic cylinder. The experimental setup is shown in Figure 13. The DC motor was used to control the cam. The pneumatic cylinder used in the experiment had an inner diameter of 10 mm and stroke of 30 mm (SMC CJ2XB10-30Z). A load of 69.5 g was mounted on the rod tip of the cylinder. Supply pressure was set to 500 kPa. One chamber of the cylinder was kept at a constant pressure of 200 kPa, while the other chamber was controlled by the servo valve.

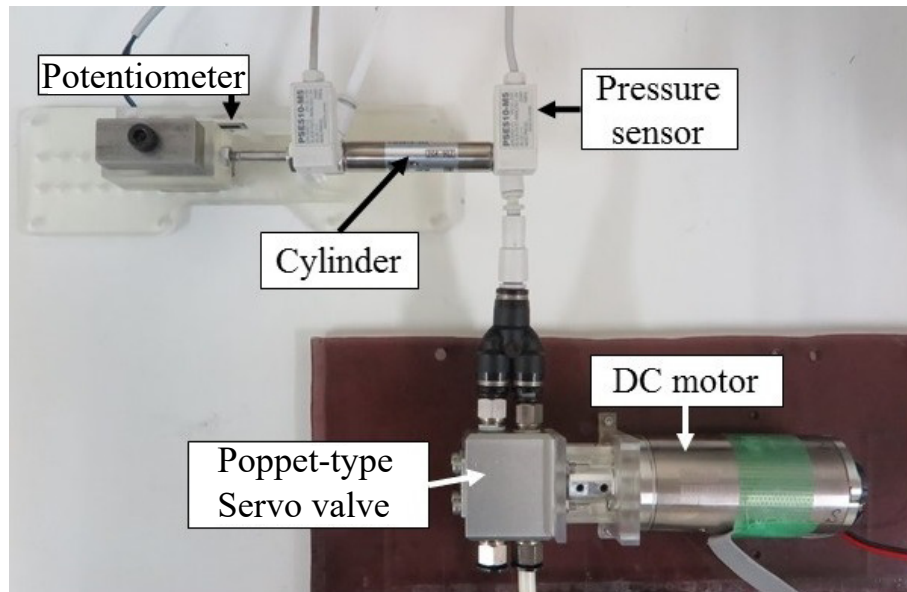


Figure 13. Experimental setup of position control.

A block diagram of the position control is shown in Figure 14. A cascade control was designed. The main loop was a PID position control, and the minor loop was a PI pressure control. The control parameters listed in Table 4 were determined experimentally.

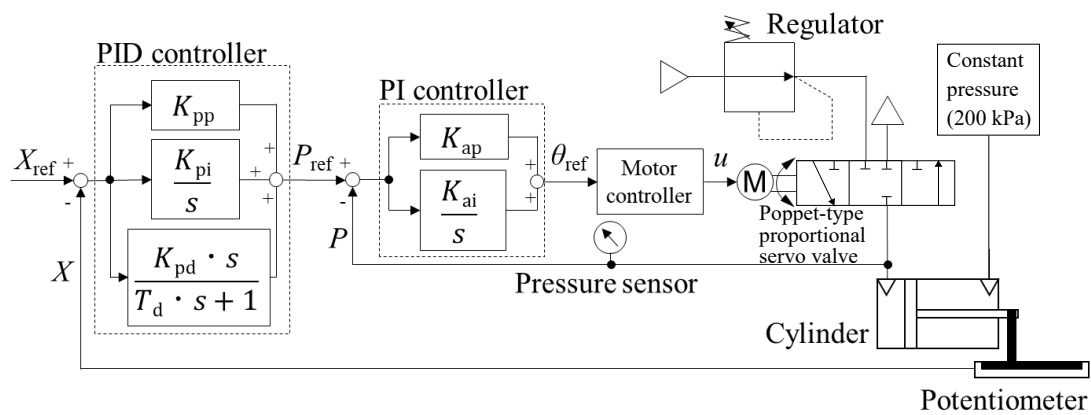


Figure 14. Block diagram of position control.

Table 4. Control gains of position control.

K_{pp}	38 kPa/mm
K_{pi}	1.5 kPa/mm s
K_{pd}	0 kPa s/mm
K_{ap}	0.25 V/kPa
K_{ai}	0.12 V/kPa s

Experimental results for sinusoidal input are shown in Figure 15, corresponding to frequencies of 0.5 and 2 Hz. The upper figure shows the position-tracking performance, the middle figure shows the pressure, and the lower figure shows the movement of the cam. We confirmed that the valve is effective for the position control of pneumatic cylinders.

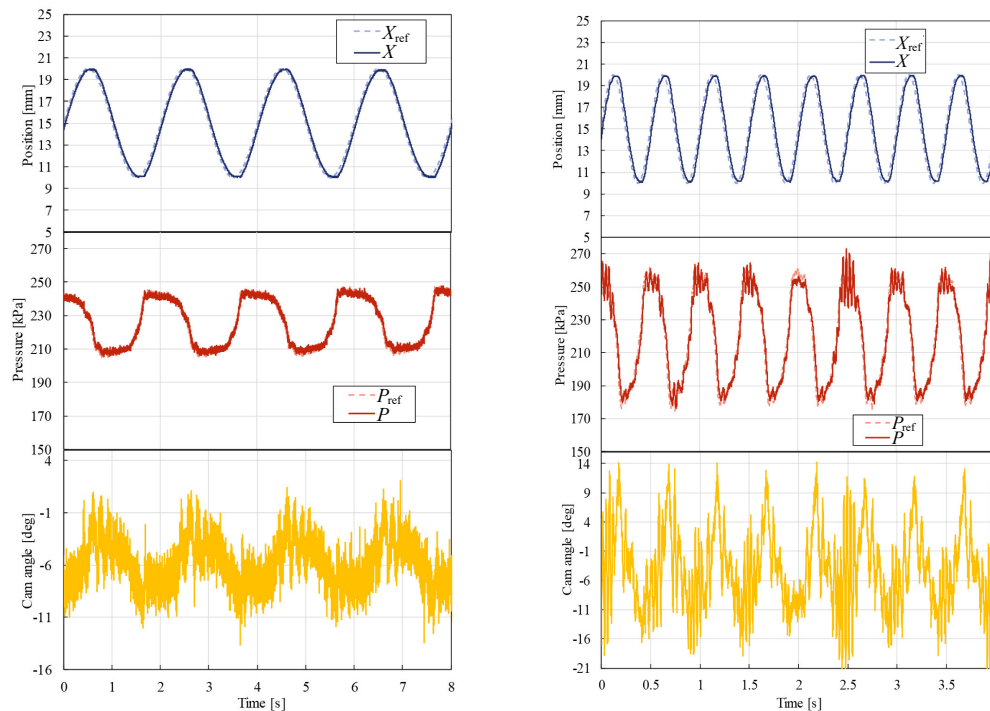


Figure 15. Position control results (left: 0.5 Hz right: 2.0 Hz).

5. Conclusions

We developed a three-port poppet-type servo valve for the purpose of reducing air leakage in pneumatic valves. In the valve, two resin orifices were placed in the flow channels of the valve, and a metal ball pushed to the orifice shut off air flow. The port was opened when the camshaft was rotated, and the cam at the downstream side of the orifice pushed the ball. Cam shape and orifice size were designed to have the desired maximum flow rate. A DC motor, having been selected based on the required torque, was employed to rotate the camshaft. The static and dynamic characteristics of the valve were measured. We confirmed from the flow characteristics that air leakage was 0.1 L/min or less. The ratio of air leakage to maximum flow rate was only 0.37% with the developed valve. Dynamic characteristics measurements showed that valve bandwidth was at least 30 Hz. Finally, the effectiveness of the valve was demonstrated through pressure and position-control experiments.

Future work will involve improving the dynamic response by using a high-response DC motor and by changing the O-ring. In addition, we intend to examine the durability of the valve.

Author Contributions: conceptualization, T.K. and K.K.; methodology, T.K., T.H., T.M. and K.K.; software, T.K., T.H., and T.M.; validation, T.H., T.M., and N.Y.; formal analysis, N.Y. and D.H.; investigation, T.M. and K.K.; resources, D.H. and K.K.; data curation, T.K.; writing—original draft preparation, T.K. and K.K.; writing—review and editing, T.K. and K.K.; visualization, T.K. and T.H.; supervision, K.K.; project administration, D.H. and K.K.; funding acquisition, K.K.

Funding: This research was funded by RiverField Inc.

Conflicts of Interest: The authors declare no conflict of interest.

References

1. Krivts, I.L. Optimization of performance characteristics of electro pneumatic two-stage servo valve. *J. Dyn. Syst. Meas. Control* **2004**, *126*, 416–420. [[CrossRef](#)]
2. Belforte, G.; Mauro, S.; Mattiazo, G. A method for increasing the dynamics performance of pneumatic servo systems with digital valves. *Mechatronics* **2004**, *14*, 1105–1120. [[CrossRef](#)]
3. Miyajima, T.; Fujita, T.; Sakaki, K.; Kawashima, K.; Kagawa, T. Development of a digital control system for high-performance pneumatic servo valve. *Precis. Eng.* **2007**, *31*, 156–161. 2006.05.003. [[CrossRef](#)]

4. Li, J.; Choi, J.; Kawashima, K.; Fujita, T.; Kagawa, T. Integrated control design of pneumatic servo table considering the dynamics of pipelines and servo valve. *Int. J. Autom. Technol.* **2011**, *5*, 485–492. [[CrossRef](#)]
5. Kawashima, K.; Youn, C.; Kagawa, T. Development of a Nozzle-Flapper Type Servo Valve Using a Slit Structure. *J. Fluid Eng.* **2007**, *129*, 573–578. [[CrossRef](#)]
6. Kagawa, T. Heat Transfer Effects on the Frequency Response of a Pneumatic Nozzle Flapper. *J. Dyn. Syst. Meas. Control* **1985**, *107*, 332–336. [[CrossRef](#)]
7. Kamali, M.; Jazayeri, S.A.; Najafi, F.; Kawashima, K.; Kagawa, T. Integrated nozzle-flapper valve with piezoelectric actuator and isothermal chamber: A feedback linearization multi control device. *J. Mech. Sci. Technol.* **2016**, *30*, 2293–2301. [[CrossRef](#)]
8. Liu, S.; Bobrow, J.E. An analysis of a pneumatic servo system and its application to a computer-controlled robot. *J. Dyn. Syst. Meas. Control* **1988**, *110*, 228–235. [[CrossRef](#)]
9. Pu, J.; Weston, R.H. A new generation of pneumatic servo for industrial robot. *Robotica* **1989**, *7*, 17–24. [[CrossRef](#)]
10. Haraguchi, D.; Kanno, T.; Tadano, K.; Kawashima, K. A Pneumatically-Driven Surgical Manipulator with a Flexible Distal Joint Capable of Force Sensing. *IEEE/ASME Trans. Mechatron.* **2015**, *20*, 2950–2961. [[CrossRef](#)]
11. Uehara, S.; Hirai, S. Unconstrained Vibrational Pneumatic Valves for Miniaturized Proportional Control Devices. In Proceedings of the 9th International Conference Mechatronics Technology, Kuala Lumpur, Malaysia, 5–8 December 2005.
12. Akagi, T.; Dohta, S.; Katayama, S. Development of Small-Sized Flexible Pneumatic Valve Using Vibration Motor and Its Application for Wearable Actuator. In Proceedings of the 15th International Conference Mechatronics Machine vision Practice, Auckland, New Zealand, 2–4 December 2008; pp. 441–446.
13. Nasir, A.; Akagi, T.; Dohta, S.; Ono, A. Analysis of Low-cost Wearable Servo Valve Using Buckled Tubes for Optimal Arrangement of Tubes. In Proceedings of the IEEE International Conference on Advanced Intelligent Mechatronics, Busan, Korea, 7–11 July 2015; pp. 830–835.
14. Morisaki, D.; Kanno, T.; Kawashima, K. Development of a Pinch-type Servo Valve Embedded in a Pneumatic Artificial Rubber Muscle. In Proceedings of the IEEE/SICE International Symposium on System Integration, Taipei, Taiwan, 11–14 December 2017.
15. Carneiro, J.F.; de Almeida, F.G. Using two servovalves to improve pneumatic force control in industrial cylinders. *Int. J. Adv. Manuf. Technol.* **2013**, *66*, 283–301. [[CrossRef](#)]
16. Kawashima, K.; Arai, T.; Tadano, K.; Fujita, T.; Kagawa, T. Development of Coarse/Fine Dual Stages using Pneumatically Driven Bellows Actuator and Cylinder with Air Bearings. *Precis. Eng.* **2010**, *34*, 526–533. [[CrossRef](#)]
17. Kawashima, K.; Ishii, Y.; Funaki, T.; Kagawa, T. Determination of Flow Rate Characteristics of Pneumatic Solenoid Valves Using an Isothermal Chamber. *J. Fluid Eng.* **2004**, *126*, 273–279. [[CrossRef](#)]
18. Andersen, B.W. *The Analysis and Design of Pneumatic Systems*; Krieger Publishing Company: Malabar, FL, USA, 2010.
19. Takosoglu, J.; Laski, P.; Blasiak, S.; Bracha, G.; Pietrala, D.; Zwierzchowski, J.; Nowakowski, L. Determination of flow-rate characteristics and parameters of piezo pilot valves. *EPJ Web Conf.* **2017**, *143*, 02126. [[CrossRef](#)]

